Bulletin of the Seismological Society of America, Vol. 82, No. 2, pp. 1071–1098, April 1992

FREQUENCY LIMITS FOR SEISMOMETERS AS DETERMINED FROM SIGNAL-TO-NOISE RATIOS. PART 1. THE ELECTROMAGNETIC SEISMOMETER

By Peter W. Rodgers

Abstract

The range of frequencies that a seismometer can record is nominally set by the corner frequencies of its amplitude frequency response. In recording pre-event noise in very quiet seismic sites, the internally generated self-noise of the seismometer can put further limits on the range of frequencies that can be recorded. Some examples of such low seismic noise sites are Lajitas, Texas; Deep Springs, California; and Karkaralinsk, U.S.S.R. In such sites, the seismometer self-noise can be large enough to degrade the signal-to-noise ratio (SNR) of the recorded pre-event data. The widely used low seismic noise model (LNM) (due to Peterson, 1982; Peterson and Hutt, 1982; Peterson and Tilgner, 1985; Peterson and Hutt, 1989) is used as representative of the input ground motion acceleration power density spectrum (pds) at such very low noise sites.

This study determines the range of frequencies for which the SNR of an electromagnetic seismometer exceeds 3 db (a factor of 2 in power and 1.414 in amplitude). In order to do this, an analytic expression is developed for the SNR of a generalized electromagnetic seismometer. The signal pds using Peterson's LNM as an input is developed for an electromagnetic seismometer. Suspension noise is modeled following Usher (1973). In order to determine the electronically caused component of the self-noise, noise properties are compared among three commonly used amplifiers. The advantages and disadvantages of the inverting and noninverting configurations in terms of their SNR are discussed. In most cases, the noninverting configuration is to be preferred as it avoids the use of the large gain setting resistances required in the inverting configuration to avoid loading the seismometer output. A noise model is developed for a typical low noise operational amplifier (Precision Monolithics OP-27). This noise model is used to numerically compute the SNRs for the three electromagnetic seismometers used as examples. The degradation in SNR caused by large gain setting resistances is shown.

Numerical examples are given using the Mark Products L-4C and L-22D and the Teledyne Geotech GS-13 electromagnetic seismometers. For each of the example seismometers, the calculated range of frequencies for which their SNR exceeds 3 db is as follows: the GS-13, 0.078 to 56.1 Hz; the L-4C, 0.113 to 7.2 Hz; and the L-22D, 0.175 to 0.6 Hz. For the GS-13, the calculated lower and upper frequencies at which the SNR is 3 db are 0.078 and 56.1 Hz. This compares with the values 0.073 and 59 Hz measured in the noise tests on the vertical GS-13.

Expressions for the total noise voltage referred to the input of an operational amplifier are developed in Appendix A. It is shown that in the inverting configuration, although no noise current flows in the input resistor, the noise current appears in the expression for the total noise voltage as if it did. In Appendix B, it is shown that any noise current flowing through an electromagnetic seismometer having a generator greater than several hundred V / m / sec generates a back emf that adds significantly to the noise of the system. This implies that system noise tests that substitute a resistor at the noninverting input of the preamplifier or clamp the seismometer mass will tend to underestimate the system noise.

Introduction

In general, the range of frequencies over which a seismometer operates is set by the nominal values of the corner frequencies of its amplitude frequency response, which is to say its passband. For an electromagnetic seismometer, the nominal low frequency limit, or corner frequency, is set by the free period of the spring-mass system, and the high frequency corner is usually set by a low-pass filter following the seismometer. In very low noise sites, the seismometer's internally generated noise together with the noise associated with the preamplifier can compete with the signal due to ground motion. This self-noise of the seismometer and amplifier also sets limits on the range of frequencies that the seismometer can record with fidelity. This is a particularly significant problem in recording in very low noise seismic sites where the ground motions are exceedingly small, of the order of tenths of nanometers of displacement and nano-*g*s of acceleration. Examples of such sites are Lajitas, Texas (Li *et al.*, 1984); RSNT in the Northwest Territories (Rodgers *et al.*, 1987); Karkaralinsk in the U.S.S.R. (Berger *et al.*, 1988); and Deep Springs, California (Gurrola *et al.*, 1990).

The approach taken in treating this problem for the electromagnetic seismometer is to determine the range of frequencies for which the seismometer signal due to ground motion exceeds that due to the self-noise of the seismometer and preamplifier. Since it is often desirable to resolve the ambient background signal preceding an event, this pre-event noise is used as the ground motion input signal to the seismometer. The sources of seismometer self-noise considered are the suspension noise, the Johnson noise from the coil and damping resistors, and the electronic noise from the preamplifier, all of which are well characterized. In order to make the problem at least tractable, less well-characterized noise sources such as cross-axis sensitivity, parametric effects (Rodgers, 1975), suspension resonances, and nonlinearities are not treated here, not that they are unimportant. Certainly suspension resonances limit the upper frequency range of seismometers, but in well designed suspensions this usually occurs at higher frequencies than are being treated here. Apparently the omissions are not of great consequence, as the results appear to correspond to measured data reasonably well.

Seismic Ground Motion Model

The seismic ground motion used as an input to the seismometer in this study is the seismic noise that precedes the event. It will be required that the signal resulting from this input exceed the internal, or self-noise, of the seismometer and preamplifier so that this pre-event noise can be recorded accurately. The seismic noise model used is that developed over a number of years by Jon Peterson (Peterson, 1982; Peterson and Hutt 1982; Peterson and Tilgner, 1985; Peterson and Hutt, 1989) of the Albuquerque Seismic Laboratory (ASL). This model represents the ambient seismic background noise at the very quietest borehole sites. It is an amalgam of long- and mid-period low seismic noise from SRO and ASRO stations with high-frequency low-noise data from Lajitas, Texas (Li *et al.*, 1984). The resulting low-noise model (hereafter called the LNM) is a standard by which seismometers may be evaluated and compared. Of course, the results developed here are dependent on this noise model, but the LNM has been widely accepted. It was recommended as a standard by the workshop on

Standards for Seismometer Testing held at ASL in July 1989. At least three manufacturers (Guralp Systems, Ltd., Quanterra, Inc., and Kinemetrics, Inc.) regularly include the LNM with their plots of seismometer self-noise.

Peterson's LNM is shown in Figure 1. It covers the range 1000 sec to 100 Hz. The ordinates are acceleration power density spectra (acceleration pds), which have the units mean squared acceleration per Hz. All the pds's used in this study have the units mean squared amplitude per Hz. The principle feature of the LNM is a large microseismic peak near 0.2 Hz. Below this is the low-frequency minimum near 0.015 Hz. Above 1 Hz, the spectrum is almost a constant out to 100 Hz. As will be shown, it is this range that challenges seismometers.

In order to appreciate how low the accelerations actually are in this model, the LNM is shown again in Figure 2, but in units of ground acceleration (non spectral density units). The acceleration units used in Figure 2 are average peak-to-peak acceleration in a 1/2 octave bandwidth. Average peak-to-peak values are twice the rms values (Aki and Richards, 1980; Taylor, 1981). The rms values are obtained from

$$\text{rms} = \sqrt{2 \cdot BW(f) P_{aa}(f)}\,, \tag{1}$$

where the $1/n$ octave bandwidth, $BW(f)$, is given by

$$BW(f) = (2^{1/n} - 2^{-1/n}) \cdot f \tag{2}$$

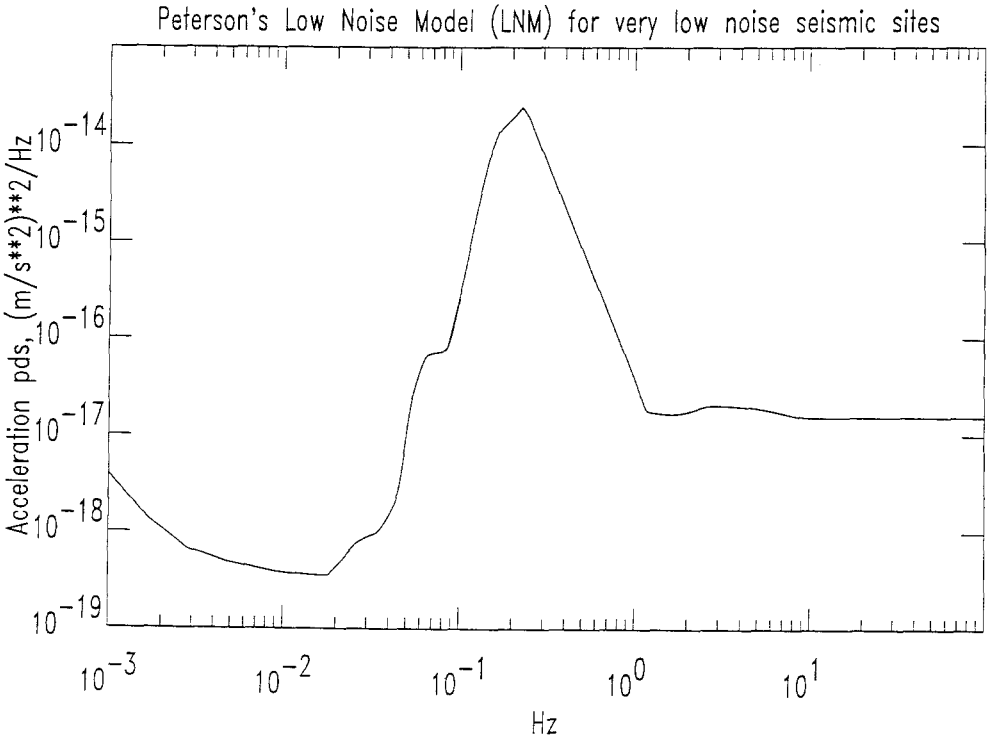

FIG. 1. Low seismic noise models (LNM) power density spectrum (pds) from 0.001 to 100 Hz (Peterson, 1982; Peterson and Tilgner, 1985; Peterson and Hutt, 1989). The ordinates are in mean squared acceleration power density. A prominent microseism peak appears near 0.2 Hz. The acceleration pds is nearly constant from 1 to 100 Hz.

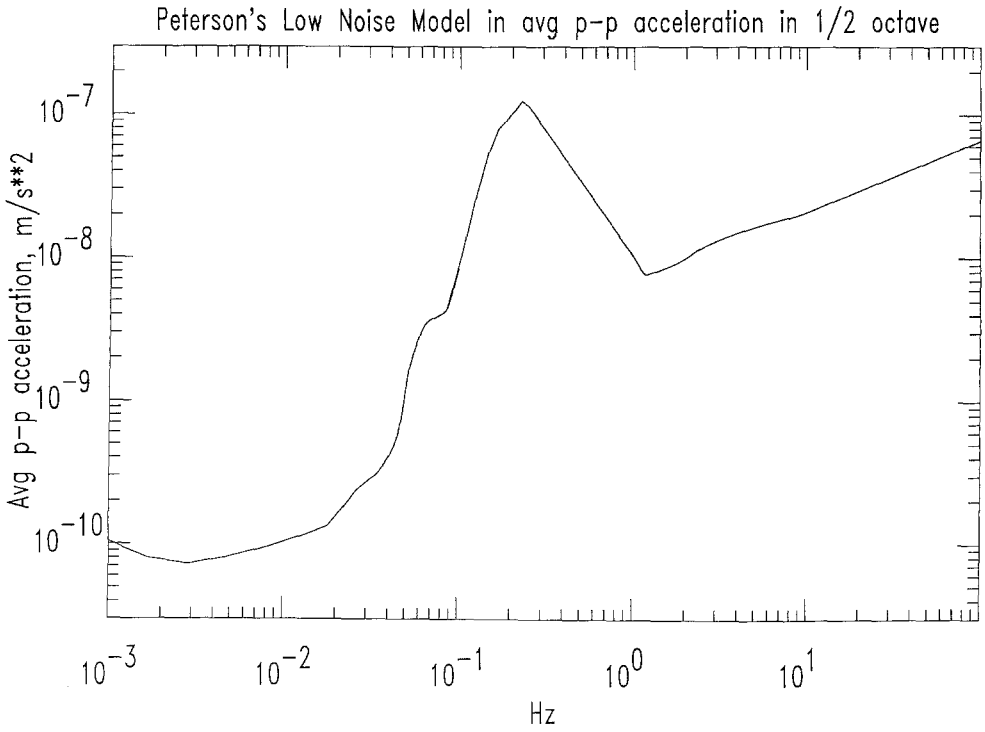

FIG. 2. Peterson's low seismic noise model (LNM) replotted with ordinate units of average peak-to-peak acceleration in 1/2 octave bandwidth. The dip near 1 Hz corresponds approximately to 1 nano-g.

(Aki and Richards, 1980; Papoulis, 1965). For a one-half octave bandwidth, $n = 2$. As can be seen, the acceleration level at 1 Hz is approximately a nano-g. However, the calculations in this paper will be carried out using the pds data of Figure 1.

SUSPENSION NOISE MODEL

The suspension noise of a spring-mass system is due to the Brownian motion of its mass. The resulting acceleration power density spectrum (acceleration pds) of the suspension noise, S_{nn}, is a constant and is given by equation (3), which can be derived from the expression for suspension noise given by Aki and Richards (1980).

$$S_{nn} = 16\frac{\pi k T \zeta f_0}{M} \qquad (\mathrm{m/sec^2})^2/\mathrm{Hz}, \tag{3}$$

where S_{nn} = suspension noise acceleration pds in $(\mathrm{m/sec^2})^2/\mathrm{Hz}$; k = Boltzmann's constant = 1.38×10^{-23} joules/°K; T = room temperature in °K = 293°K; ζ = damping ratio of spring-mass system; M = mass in kg; and f_0 = resonant frequency of spring-mass system in Hz.

Of the three seismometers used as examples in this paper, only in the Mark Products L-22D does the suspension noise become a significant fraction of the total noise. This is because of its relatively light mass of 0.0728 kg and large damping ratio of 0.8. In the analysis that follows, the suspension noise will be retained for generality even if it is negligible for a particular seismometer.

Electronic Noise Models

Three types of electronic noise are treated in this section: Johnson or thermal noise, and the voltage noise and the current noise produced at the input of an operational amplifier that uses bipolar transistors or field effect transistors (FETs). These noises are given in terms of voltage power density spectra (voltage pds), which have the units mean squared volts per Hz. Much of this material is treated by Horowitz and Hill (1990, Chapter 7) and Vergers (1987).

Johnson Noise

The Johnson or thermal noise is the random voltage produced across a resistance by the thermal agitation of electrons. The voltage pds of Johnson noise is given by

$$J_{nn} = 4kTR \qquad (\mathrm{V}^2/\mathrm{Hz}), \tag{4}$$

where J_{nn} = Johnson noise pds in V^2/Hz; k = Boltzmann's constant = 1.38×10^{-23} joules/°K; T = room temperature in °K = 293°K; and R = resistance in ohms. With these values, equation (4) becomes

$$J_{nn} = 1.617 \times 10^{-20} R \qquad (\mathrm{V}^2/\mathrm{Hz}). \tag{5}$$

That Johnson noise is a significant part of electronic noise can be seen from equation (5), where for a resistance as small as 0.5 k-ohm, the Johnson noise is 8.09×10^{-18} V^2/Hz. It will be seen that this nearly equals the voltage noise at the input of a low noise operational amplifier, and it is one of the reasons for keeping circuit resistances as low as possible.

Voltage and Current Noise Models

Solid state components such as operational amplifiers and FETs generate both voltage and current noise at their inputs. There is a large variation in these properties between types (and also between units of the same type). For example, a FET or FET operational amplifier is characterized by very low current noise and fairly high voltage noise compared to a bipolar operational amplifier. The electronic noise generated by both types is treated.

In choosing a low noise operational amplifier to serve as a representative noise model for this study, data from six major manufacturers were reviewed. These were Analog Devices, Burr-Brown, Linear Technology, National Semiconductor, Precision Monolithics, and Signetics. Although all of these manufacturers list low noise operational amplifiers in their literature, for only a few amplifiers are sufficient data given on which to base a noise model. Three were chosen to use as representative examples here. They are the Linear Technology's LT1028 and the Precision Monolithics OP-27 and MAT-02, which is a matched bipolar transistor pair having the characteristics similar to a FET. Also considered were the Burr-Brown OPA2111 FET operational amplifier, the National Semiconductor LM312 (similar to the Precision Monolithics OP-12), and the Analog Devices AD705. These latter two were not used because, for the range of source resistances considered here, they were clearly more noisy than the three selected. A summary of the voltage and current noise characteristics of six low noise operational amplifiers is given by Riedesel *et al.*, (1990).

The total electronic noise, E_{nn}, appearing at the input of a preamplifier based on an operational amplifier is given by equation (6). In Appendix A, it is shown that this equation is valid for both the inverting and noninverting operational amplifier configurations when the gain is at least moderately greater than one.

$$E_{nn} = V_{nn} + I_{nn}R^2 + J_{nn} \qquad (\mathrm{V}^2/\mathrm{Hz}), \tag{6}$$

where E_{nn} = total electronic noise voltage pds appearing at input to preamplifier in V^2/Hz; V_{nn} = voltage noise pds at inverting terminal in V^2/Hz; I_{nn} = noise current pds in A^2/Hz for noise current flowing from the inverting terminal (it is assumed that the noise current flowing from the non-inverting terminal is identical). R = input or source resistance in ohms (for the inverting configuration, R is the total input resistance; for the noninverting configuration, R is the source resistance in series with the parallel combination of the gain setting resistances, equation (29-A), Appendix A); and J_{nn} = Johnson or thermal noise generated due to the resistances in the circuit (J_{nn} is different for the inverting and noninverting configurations; the expressions for each are given in Appendix A).

In the inverting configuration, no noise current flows through the input resistance, R (Tobey *et al.*, 1971; Riedesel *et al.*, 1990). Nevertheless, it is shown in Appendix A that, because of the gain action of the operational amplifier, I_{nn} is multiplied by a gain term resulting in the expression $I_{nn}R^2$ in E_{nn}. It will be seen later that this term has a major effect on the signal-to-noise ratio of the seismometer and preamplifier combination.

Based on the manufacturer's data on the OP-27 operational amplifier, models for the voltage and current noise power density spectra (pds) were constructed as follows:

$$V_{nn} = 9\left(\frac{2.7}{f} + 1\right) \times 10^{-18} \qquad (\mathrm{V}^2/\mathrm{Hz}), \tag{7}$$

$$I_{nn} = 0.16\left(\frac{140}{f} + 1\right) \times 10^{-24} \qquad (\mathrm{A}^2/\mathrm{Hz}). \tag{8}$$

In these models, f is the frequency in Hz. Both the voltage and current noises have a corner frequency, the numerator of f, and rise with a -1 slope as frequency decreases. This is due to the flicker or $1/f$ noise (Horowitz and Hill, 1990) and will be seen to be a factor that limits the low-frequency or long-period response of a seismometer. The voltage noise is referred to virtual ground. Similar models were used by Riedesel *et al.*, (1990). Using these models for the OP-27, Figure 3 plots the three terms (V_{nn}, $I_{nn}R^2$, and J_{nn}) in equation (6) together with the total noise, E_{nn} (upper, solid curve), versus frequency for a source resistance, R = 2k ohms. As can be seen, the Johnson noise dominates above 3 Hz, whereas the current noise dominates for frequencies below 3 Hz. This shows the importance of keeping the source resistance low since both the current and Johnson noise depend on it. The deleterious effect of a large source resistance on the seismometer frequency limits will be seen in more detail later.

The reason for selecting the OP-27 for the representative noise model is shown in Figure 4, which plots the total electronic noise, E_{nn}, for the LT1028, the MAT-02, and the OP-27 for source resistances, R, of 2k and 50k ohms.

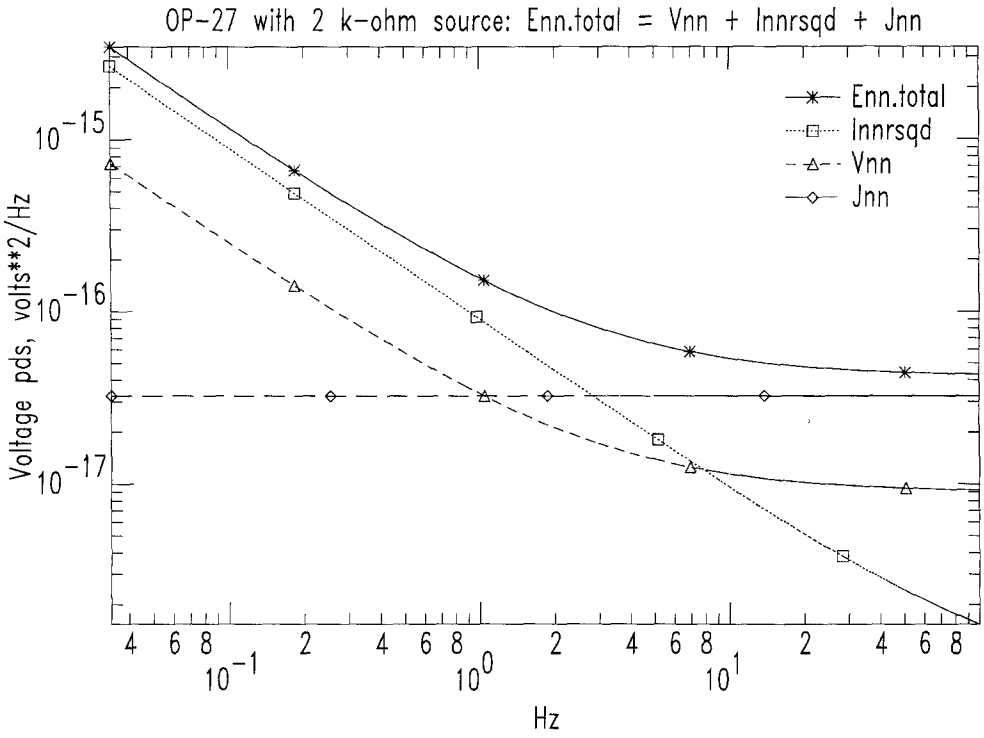

FIG. 3. Four noise voltage pds models for the Precision Monolithics OP-27 operational amplifier with a 2 kilo-ohm source resistance. Shown are the Johnson (thermal) noise, Jnn; the voltage noise, Vnn; the voltage noise resulting from current noise, Innrsqd; and the total electronic noise, Enn. total, which is the sum of the three. These calculations were made using the non-inverting configuration assuming that the gain setting resistances are much smaller than the source resistance.

Clearly, for the 2k-ohm source resistance the OP-27 is the quietest (bottom, solid curve). For the large 50k-ohm source resistance, the LT1028 is quieter, but equations (5) and (6) show that preamplifier performance will always be improved by keeping the source resistance low. This paper will assume that as low a source resistance as possible is used, and it will compare seismometer signal-to-noise-ratios using both bipolar and FET operational amplifiers under that assumption.

THE ELECTROMAGNETIC SEISMOMETER

Analysis

The electromagnetic (E-M) seismometer utilizes a coil and magnetic pair to transduce the mass velocity into a voltage. This voltage is usually quite small and therefore requires a preamplifier to elevate it to a useful level suitable for filtering or digitizing. The most common configuration is illustrated in Figure 5, which shows the E-M seismometer on the left driving an operational amplifier based preamplifier on the right. The E-M seismometer is excited by the input acceleration pds, P_{aa}. Its output appears at the terminals of its coil as shown and consists of the output signal pds, P_{ss}, due to P_{aa} plus two noise signals: the suspension noise, S_{nn}, and the Johnson noise, J_{nn}, due to its source resistance. The seismometer source resistance is the parallel combination of the

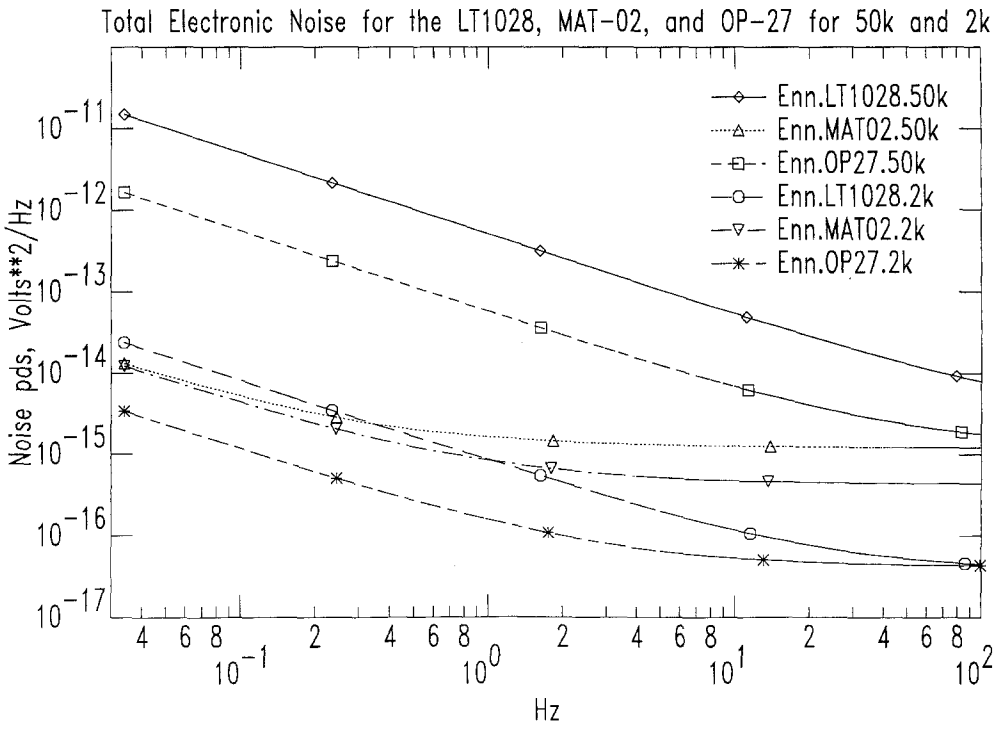

FIG. 4. Total electronic noise pds models for three amplifiers with source resistances of 2 and 50 kilo-ohms. The amplifiers are: the Linear Technologies, Inc., LT1028; the Precision Monolithics, Inc., MAT-02 and OP-27. The source resistances of 2 k- and 50 k-ohms are appended to the file names. These calculations were made using the noninverting configuration assuming that the gain setting resistances are much smaller than the source resistance.

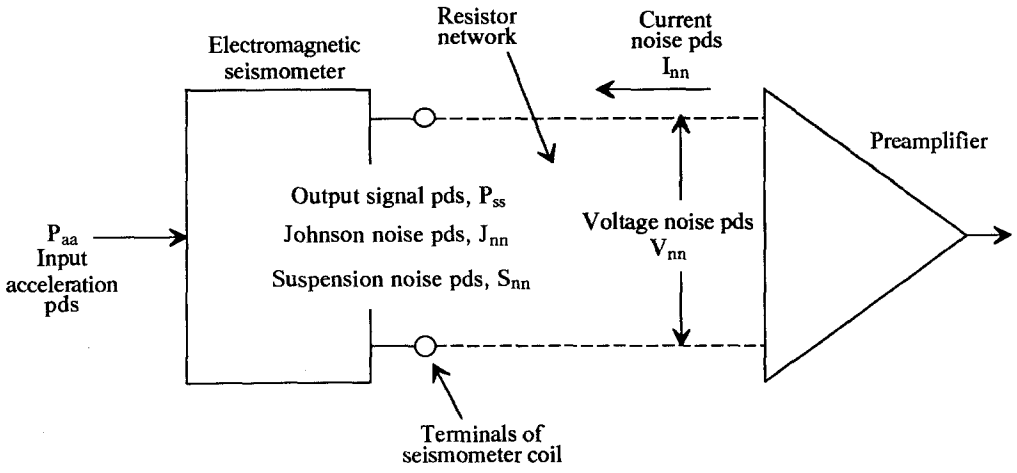

FIG. 5. The configuration of the E-M seismometer and preamplifier pair. The seismometer input is the acceleration pds, P_{aa}, and it's outputs are the signal pds, P_{ss}, and the two noises, the suspension noise pds, S_{nn}, and the Johnson noise pds, J_{nn}. The dotted lines indicate the resistor network coupling the seismometer to the preamplifier. It is unspecified for generality. The voltage noise pds, V_{nn}, and current noise pds, I_{nn}, which appear at the input of the operational amplifier used in the preamplifier are shown.

coil and damping resistance. The seismometer coil terminals are coupled to the operational amplifier based preamplifier by an electrical network assumed to be totally resistive. As shown by equation (6), the input stage of the preamplifier adds a voltage noise pds, V_{nn}, a voltage pds, $I_{nn}R^2$, and a Johnson noise term, J_{nn}. This is the case for both inverting and noninverting configurations, which is shown in Appendix A. The coil inductance can be neglected because, for the three seismometers treated, it results in a low pass corner frequency outside the frequency range of interest. For example, even the 80 Henry inductance of the coil of the GS-13 results in a low-pass corner frequency only as low as 217 Hz.

Preamplifier Circuits

There are at least six different resistor networks that may be used to couple the output of the E-M seismometer to the preamplifier depending on whether the preamplifier input is single or double ended, whether the operational amplifiers used are connected in inverting or noninverting configurations, and whether the seismometer is close coupled or not to the preamplifier. Because of the large number of possible circuit configurations, the simplifying assumption is made that the noise currents are the same at both the inverting and noninverting inputs of the operational amplifier(s) being used. And it is also assumed that all of the voltage noise, V_{nn}, appears at the inverting terminal of the operational amplifier (Tobey *et al.*, 1971, their Appendix A). Since this paper seeks the frequency extremes that can be obtained from a seismometer, only the single-ended configuration will be treated because its noise pds due to noise currents will be half that of the corresponding double ended configuration. Of the several single-ended configurations possible, only two permit the use of very low resistances for gain setting. These are: (a) connecting the seismometer directly to the noninverting input with the damping resistor in parallel with the coil; and (b) close coupling the seismometer directly to the inverting input with a damping resistor in parallel with the coil (Teledyne Geotech, 1980). Connecting the seismometer to the inverting input directly through its damping resistor is to be avoided because it increases the source resistance by a factor of between 4 and 10. This is because the damping resistance is then in series with the coil resistance rather than in parallel with it, and damping resistances tend to be much larger than coil resistances by a factor of 3 to 9 times. What is also to be avoided from a noise point of view is to connect the seismometer to the inverting input through a large gain setting resistor or to connect the seismometer to the noninverting input and use a large gain setting resistances.

Either of the two circuits described in (a) and (b) above allow the use of low-gain setting resistances with the operational amplifier. However, because of the limited range of coil resistances, the close coupled configuration described in (b) offers less flexibility than the noninverting configuration described in (a). Based on these considerations, it is assumed in this paper that the preamplifier is based on an operational amplifier in the noninverting configuration shown in Figure A2 in Appendix A; and it is further assumed that the gain setting input resistances to the operational amplifier are low enough to be negligible compared to the seismometer resistances, so that only the seismometer resistances will be involved in the subsequent noise calculations. It may be difficult in practice to exactly implement that last assumption, but in most situations it can be achieved. In any event, it serves well as a limiting case. Assuming for the time being that there are no capacitors in the coupling network, for purposes of

the noise analysis there is a single equivalent source impedance, R, for the seismometer through which a noise current pds, I_{nn}, flows from the noninverting input. The case with capacitors will be discussed later.

SNR of the Electromagnetic Seismometer

To make the analysis explicit for the signal and noise for the E-M seismometer, a block diagram of the configuration is shown in Figure 6. In this figure the input acceleration pds, P_{aa}, and suspension noise pds, S_{nn}, are shown passing through the seismometer separately. This is done to separate out the seismometer output signal, P_{ss}, due to the input acceleration pds, P_{aa}. S_{nn} and E_{nn} are realistically assumed to be independent. The resulting signals are summed together with the total electronic noise pds, E_{nn}, to produce the output voltage pds, P_{yy}, which is referred to the input of the preamplifier. The input and output power density spectra (pds) for the E-M seismometer are related by the term $|H(\omega)|^2$, which is defined as

$$|H(\omega)|^2 = \left[\frac{r_d}{r_c + r_d} G\right]^2 \cdot \frac{\omega^2}{\left(\Omega^2 - \omega^2\right)^2 + 4\zeta^2\Omega^2\omega^2} \qquad \left(\frac{\mathrm{V}^2/\mathrm{Hz}}{\left(\mathrm{m/sec}^2\right)^2/\mathrm{Hz}}\right), \quad (9)$$

where $H(\omega)$ = the Fourier transfer function of the seismometer in V/m/sec^2, which is the acceleration sensitivity; ω = angular frequency in radians/sec = $2\pi f$ with f in Hz; r_d = damping resistor in ohms; r_c = coil resistance in ohms; G = generator constant (unloaded) in V/m/sec; Ω = angular resonant frequency of the spring-mass system = $2\pi f_0$, where f_0 is the seismometer resonant frequency; and ζ = damping ratio.

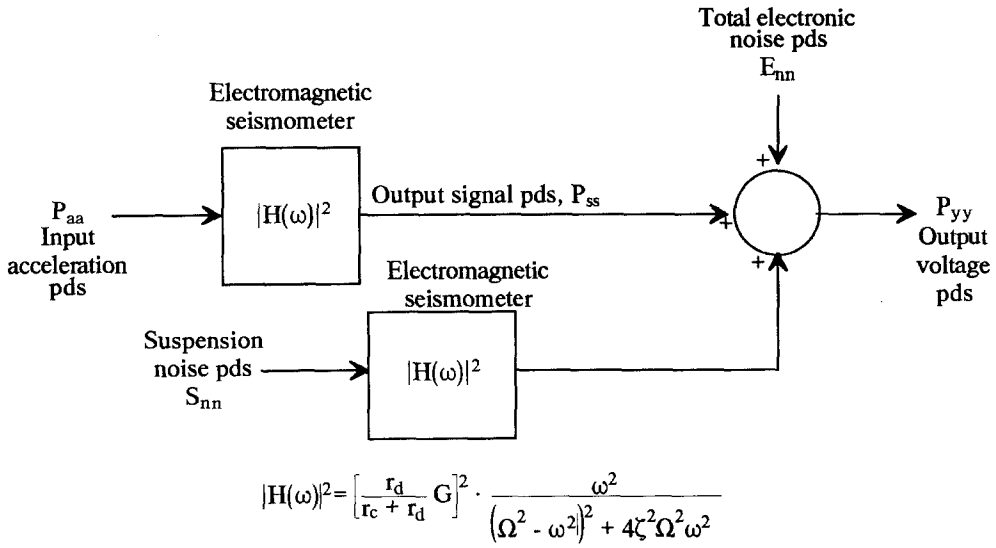

FIG. 6. Block diagram for signal and noise analysis of the E-M seismometer/preamplifier combination. The input is the acceleration pds, P_{aa}, and its signal output is P_{ss}. The voltage noise due to the suspension noise, S_{nn}, and the total electronic noise, E_{nn}, are added into the bottom and top of the summing point, respectively. The output of the summing point is the voltage pds, P_{yy}, which is referred to the preamplifier input. The output, P_{yy}, is composed of a signal part, P_{ss}, due to P_{aa} and a noise part, P_{nn}, due to S_{nn} and E_{nn}. The E-M seismometer Fourier transform transfer function is $H(\omega)$ in units of V/m/sec^2. The parameters of the transfer function are defined in the body of the text.

The output voltage pds, P_{yy}, is the sum of the signal pds, P_{ss}, and the noise pds, P_{nn}:

$$P_{yy} = P_{ss} + P_{nn} \qquad (\mathrm{V}^2/\mathrm{Hz}), \tag{10}$$

where P_{yy} = output voltage pds, in P_{ss} = signal pds, and P_{nn} = noise pds all in V^2/Hz). The signal pds is obtained from the input acceleration pds by means of equation (11) (Aseltine, 1958; Papoulis, 1965):

$$P_{ss} = |H(\omega)|^2 \cdot P_{aa}, \qquad \mathrm{V}^2/\mathrm{Hz} \tag{11}$$

where P_{aa} = the input acceleration pds in $(\mathrm{m/sec}^2)^2/\mathrm{Hz}$ and P_{ss} = the signal pds in V^2/Hz.

As indicated in Figure 6, the noise pds, P_{nn}, is obtained by summing the total electronic noise pds, E_{nn}, with the seismometer output due to suspension noise. The results in equation (12):

$$P_{nn} = E_{nn} + |H(\omega)|^2 S_{nn}. \qquad \mathrm{V}^2/\mathrm{Hz} \tag{12}$$

All the terms in equation (12) have been previously defined. Finally, using equations (11) and (12), the signal-to-noise-ratio (SNR) for the E-M seismometer is obtained:

$$\mathrm{SNR}_{\mathrm{em.seis}} = \frac{P_{ss}}{P_{nn}} = \frac{|H(\omega)|^2 \cdot P_{aa}}{E_{nn} + |H(\omega)|^2 S_{nn}}. \tag{13}$$

The total electronic noise, E_{nn}, is computed using equation (6) with R^2 replaced by $|Z_s|^2$ because, for the noninverting configuration, the noise current flows through the seismometer and not a simple resistance. The expression for $|Z_s|^2$ is derived in Appendix B. When the noise current, or some fraction of it if there is a damping resistor, flows into the seismometer it exerts a force on the mass equal to Gi, where i is the current flowing through the coil. This force causes the seismometer mass to move with respect to the frame, generating a back electro-motive-force or emf, increasing E_{nn}. For seismometers having large generator constants, this back emf may be much larger than the voltage drop across R and so must be accounted for in computing the total noise voltage, E_{nn}. In Appendix B, Figure B3 shows the total electronic noises, E_{nn}, for the GS-13 and L-4C seismometers using the OP-27 in the noninverting configuration with and without the back emf term. For the GS-13, including the back emf term increases the total electronic noise pds at 1 Hz by nearly two orders of magnitude in power. There are two ways to avoid this problem with back emf: (a) Avoid it completely by using the inverting configuration with its subsequent noise penalty because of necessarily large input resistances. There is no back emf with the inverting configuration because no noise current flows in the input resistor or the seismometer. (b) Employ a FET based operational amplifier in the noninverting configuration, relying on its low current noise to reduce the back emf effect. Numerical examples showing the effect on the SNR with and without a FET will be shown in Figure 8 later.

The back emf voltage will not appear in a clamped mass test of a seismometer with a noninverting preamplifier. Therefore, it is likely that clamped mass tests

or tests that substitute a metal film resistor for the coil and damping resistor for having seismometers with large generator constants will tend to under estimate the system noise. This will particularly be the case if the noninverting preamplifier is a bipolar operational amplifier, such as the OP-27, which has a relatively large current noise. When the preamplifier is a FET operational amplifier, which has a low current noise, eliminating the back emf by clamping the mass or substituting a resistor causes a much smaller decrease in the total electronic noise.

As mentioned earlier, the preceding analysis assumes that the coupling network between the seismometer and the preamplifier does not contain any capacitors. There are two situations in which there are capacitors used in the coupling network. In the first, a low-pass filter is included in the preamplifier to extend the low-frequency response of the E-M seismometer (Daniel, 1979; Roberts, 1989). This is done by setting the low-frequency corner of the low-pass filter to a frequency much lower than the seismometer resonant frequency, f_0. The resulting velocity sensitivity has a high-pass corner frequency at the corner frequency of the low-pass filter. If the capacitor(s) are across the feedback resistor of the first stage(s) of the preamplifier, they are essentially from input to ground for the noise current and it will flow through them. This will drop the total electronic noise for frequencies where the capacitive reactance becomes less than the equivalent source resistance, R. For example, for a 2 k-ohm source resistance and a 1 mfd capacitor, this occurs for frequencies above 80 Hz. Of course, for the lower frequencies there is no effect. The other situation in which a capacitor is used in the coupling network is when it is placed directly across the seismometer output coil terminals. This has the approximate effect of appearing to increase the seismometer mass by an amount G^2C and thus lowering the high-pass corner frequency of the velocity sensitivity response in addition to increasing the damping. In the preceding analysis, this case can be treated approximately by changing the resonant frequency, f_0, and the damping ratio, ζ, in equation (9) to their altered values and proceeding as described.

Numerical Examples

In this section, the preceding theory is applied to three frequently used E-M seismometers: the Mark Products L-4C and L-22D geophones and the Teledyne Geotech GS-13 seismometer. The instrumental parameters used for these calculations are given in Table 1.

The L-4C 1-Hz geophone is often used as a seismometer because of its relatively low (for a geophone) resonant frequency and relatively large generator constant. As a seismometer it is sometimes used to record at quiet seismic sites, and so it is reasonable to determine what its noise-dependent frequency limits are.

TABLE 1

INSTRUMENTAL PARAMETERS FOR THREE E-M SEISMOMETERS

E-M Seismometer	Resonant Frequency (f_0, Hz)	Damping Ratio (ζ)	Generator Constant (G, V/m/sec)	Mass (M, kg)	Coil Resistance (r_c, k-ohms)	Damping Resistance (r_d, k-ohms)
L-4C	1.0	0.7	275.7	1.0	5.5	8.9
L-22D	2.0	0.8	112.0	0.073	5.5	14.3
GS-13	1.0	1.0	2150.0	5.0	8.9	74.5

Figure 7 is a plot of signal and noise pds's for an L-4C as determined from equations (11) and (12), respectively. The signal is due to the LNM ground acceleration input discussed earlier. The two internal or self-noises are computed from the suspension noise together with both 4 k-ohm and 50 k-ohm source resistances appearing at the input of an OP-27 operational amplifier. The 4 k-ohm source resistance is solely due to the coil and damping resistances and assumes that the input resistances associated with the operational amplifier are very small compared to 4 k-ohms. This may be difficult to realize in some circuit situations, but it serves as a limiting case in order to determine the frequency extremes, as was mentioned earlier. With the 4 k-ohm source resistance, Figure 7 shows that the signal from the L-4C exceeds its self-noise from approximately 0.1 to 10 Hz. This agrees roughly with the results of Riedesel *et al.*, (1990), who measured a low-frequency cross-over of signal and noise at 0.05 Hz using a high-gain L-4C and a noisy site. The noisy site has the effect of increasing the pre-event signal, thus improving the seismometer frequency range. The bulge in the 4 k-ohm noise curve at 1 Hz is due to the back emf term discussed earlier. The 50 k-ohm self-noise curve is below the signal curve only

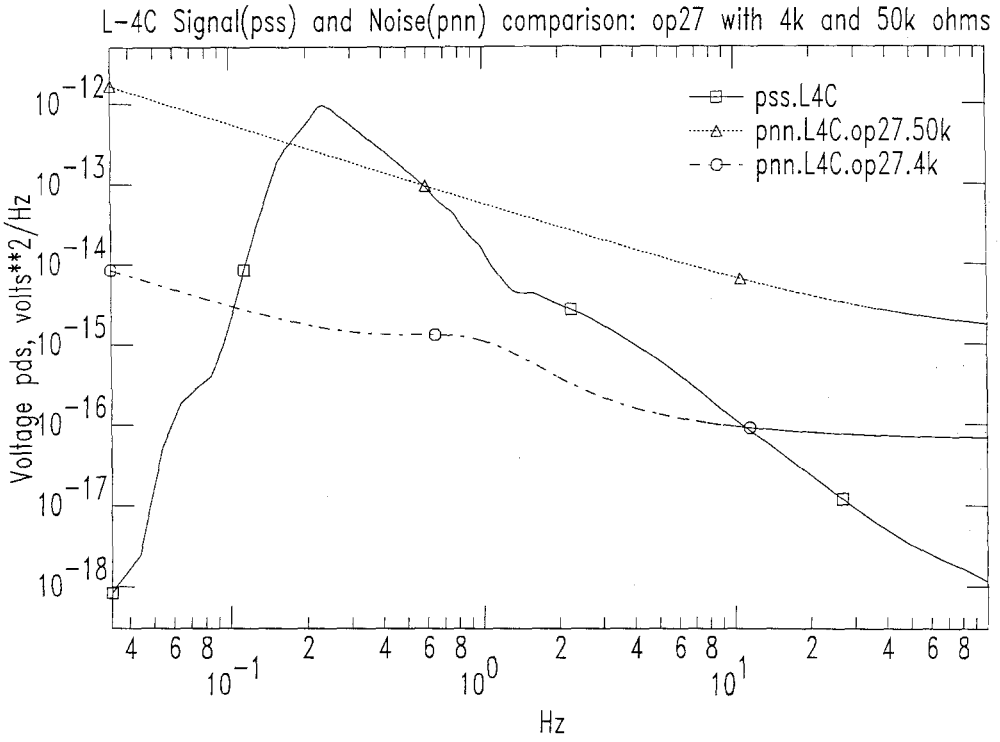

FIG. 7. Calculated signal (solid line) and noise (dotted and dashed lines) voltage pd's are plotted for the Mark Products L-4C electromagnetic seismometer. The frequency range is 0.03 to 100 Hz. Noise curves for equivalent resistances of 50 k-ohms (dotted line) and 4 k-ohms (dashed line) are shown. Where the solid line rises above the dotted or dashed lines, the signal-to-noise-ratio (SNR) > 1. This determines the frequency range over which the L-4C seismometer is able to resolve LNM pre-event noise, using the OP-27 amplifier. This figure illustrates the large decrease in useful frequency range caused by using overly large gain setting input resistances at the input of the operational amplifier-based preamplifier. The noninverting configuration was used for this calculation, and the damping resistor was in parallel with the signal coil. The rise in the noise pds for the 4 kilo-ohm curve at 1 Hz is due to the back emf generated by the motion of the mass of the seismometer being driven by the part of the noise current flowing through the signal coil.

from approximately 0.2 to 0.8 Hz. The back emf does not affect the 50 k-ohm curve because it is smaller than the voltage drop across the 50 k-ohm resistor. The point of Figure 7 is to illustrate the large decrease in useful frequency range caused by using too large a value for the input gain setting resistor. This is the case even with the inverting preamplifier configuration because of the $I_{nn}R^2$ term in the electronic noise for the inverting configuration.

Another question that the data in Figure 7 addresses is this: "To how low a frequency can the low-frequency corner of the L-4C be extended electronically?" This refers to the techniques used by Daniels (1979) and Roberts (1989). These data show that, for recording in the very quiet seismic sites represented by the LNM, about the best that can be done is 0.1 Hz. This is not to say that the low-frequency corner couldn't be electronically extended to even 0.01 Hz (100 sec), but only that there is no point in going below 0.1 Hz with the L-4C unless lower noise preamplifiers are used. For the lower frequencies, this can be achieved with chopper stabilized amplifiers.

SNRs for Three E-M Seismometers

Another useful way to examine the noise-dependent frequency limits of seismometers is to compare the signal and noise by means of the signal-to-noise-ratio (SNR). For an E-M seismometer, the SNR is given by equation (13).

Using the parameters for the three seismometers given in Table I, Figure 8 plots the SNRs for the GS-13, L-4C, and L-22D E-M seismometers over the frequency range 0.03 to 100 Hz. The preamplifier is assumed to employ a noninverting operational amplifier. For all three instruments, the OP-27 operational amplifier characteristics are used. This results in the bottom three SNR curves. In order to show the effect of changing from a bipolar to a FET operational amplifier, the SNR for the GS-13 was recalculated using the MAT-02 operational amplifier. The result is the top, solid curve for the GS-13. The large improvement in SNR is due to the decrease in back emf because of the smaller noise current of the MAT-02 compared to the bipolar OP-27. All computations were made using a source resistance approximately equal to the parallel resistance of the coil and damping resistor for each seismometer. The basis for doing this was stated in the previous section. The reference SNR is 3 db and is shown as a solid, horizontal line. Where the seismometer SNR curves intersect the 3 db line means that at that frequency the seismometer signal exceeds its self-noise by 3 db or a factor of 2 in power and a factor 1.414 in amplitude. Using the data from Figure 8, Table 2 compares the frequency ranges over which the three seismometer SNRs exceed 3 db.

The very large SNR of the GS-13 with its resulting wide frequency range (0.078 to 56.1 Hz) is due to its combination of a large generator constant (2150 V/m/sec) with a relatively low coil resistance, compared to the other two seismometers. The effect of the large generator constant is to contribute additional signal gain with no increase in electronic noise except for the small amount of Johnson noise from the coil and damping resistances. Of course, the electronic noise resulting from the suspension noise also increases with the generator constant, but because of the large mass the resulting voltage noise is negligible compared to the electronic noises at the input of the preamplifier. However, because of its large generator constant, to achieve good results with the GS-13 it is necessary to use a FET-based preamplifier in the noninverting

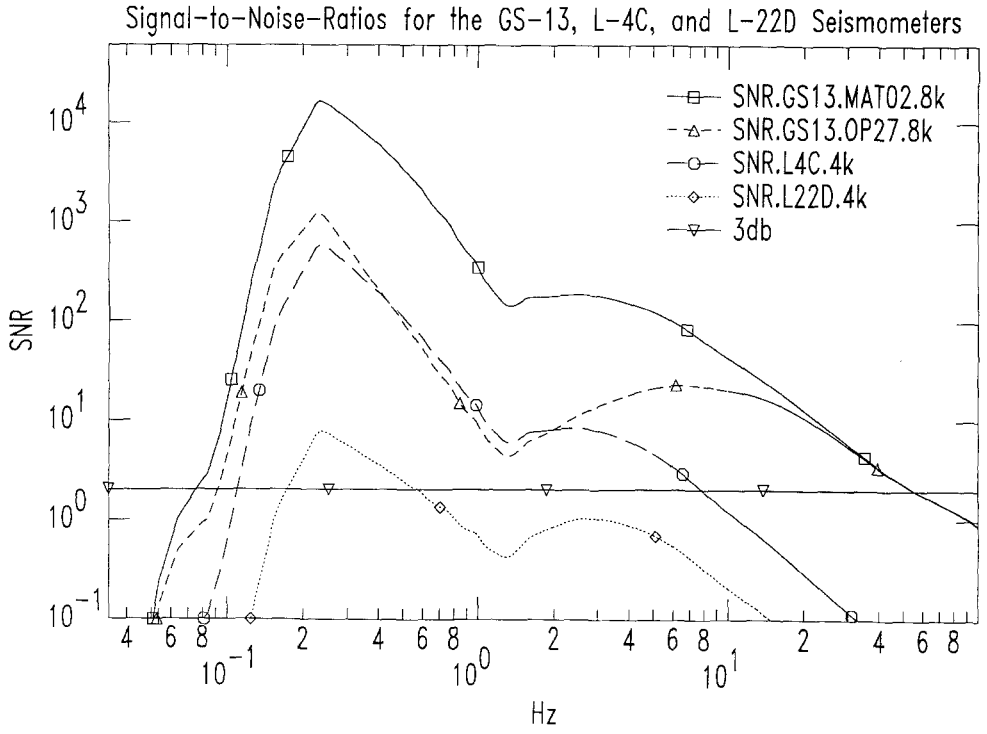

FIG. 8. Calculated signal-to-noise ratios for three E-M seismometers: the Teledyne Geotech GS-13 (solid and dot-dash curves), the Mark Products L-4C (dashed curve), and L-22D (dotted curve). The frequency range is 0.03 to 100 Hz. The horizontal solid line corresponds to a SNR of 3 db (a factor of 2 in power ratio and a factor of 1.414 in amplitude ratio). The non-inverting configuration was used for this calculation, and damping resistor was in parallel with the signal coil. The equivalent source resistances (appended to the file names) are the parallel combination of coil and damping resistance, which is the minimum possible. Where the SNR curves cross the 3 db line, the SNR = 2. This determines the frequency range over which each of the three seismometers is able to resolve LNM pre-event noise. The frequencies are given in Table 2. The upper two curves are the SNR's for the GS-13 using FET (upper, solid curve) and bipolar (lower dot-dash) operational amplifiers. The improved SNR using the FET is the result of its low noise current, which reduces the back emf generated by the large generator constant of the GS-13.

TABLE 2

FREQUENCY RANGE OVER WHICH THE SNR > 3 DB FOR THREE E-M SEISMOMETERS

E-M Seismometer	Lower Frequency (f_l, Hz)	Upper Frequency (f_u, Hz)
GS-13	0.078	56.1
L-4C	0.113	7.2
L-22D	0.175	0.6

configuration. Using the inverting configuration will degrade the SNR because of the large input resistor needed to avoid loading the 8.9 k-ohm signal coil of the GS-13.

For the GS-13, the calculated lower and upper frequencies at which the SNR is unity are 0.064 and 93.5 Hz. This compares with the values 0.06 and 57 Hz

measured in the noise tests of the vertical GS-13 (Durham, personal commun.). The method used to obtain these noise data on the GS-13 does not require clamping the mass or substituting a metal film resistor for the coil resistance, both of which tend to underestimate the noise. The method is described in detail in Appendix A of the companion paper that follows, "Frequency Limits for Seismometers as Determined from Signal-to-Noise Ratios. Part 2. The Displacement Feedback Seismometer" Rodgers (1992).

The relatively low SNR shown in Figure 8 for the L-22D is mainly due to its small generator constant (112 V/m/sec). These data indicate that the L-22D is not suitable for deployment at very low noise sites such as those represented by the LNM.

The L-4C does not cover as large a frequency range as the GS-13, but nevertheless it does well between approximately 0.1 to 10 Hz, as discussed previously.

Conclusions

This study has been an attempt remove some of the vagueness and uncertainty regarding the question of which seismometers can record satisfactorily over a given frequency range when the inputs are at a very low level. These operating frequency ranges are presented for three frequently used electromagnetic seismometers in Table 2. Finally, the study has explored the interplay between the SNR and the suspension noise, the electronic noise, the parameters of the spring-mass system, and the amplifier type. The results are qualified both because they are dependent on the various noise models used and only those issues could be addressed that are analytically tractable. Thus, effects due to cross-axis sensitivity, suspension vibrations, and parametric changes are not treated. Nevertheless, the results obtained appear reasonable and, in the cases of the L-4C and GS-13, the results match experimentally obtained data fairly well. To this extent some conclusions are warranted regarding seismometer and circuit selection for recording very low level signals:

1. The useful frequency range of electromagnetic seismometers is mainly set by their resonant frequency, generator constant, and the electronic noise of the preamplifier used. Unless the mass is very small, as in the L-22D, it does not much affect the useful frequency range.

2. It is possible to compute the SNR of electromagnetic seismometers using seismic and electronic noise models together with the instrument parameters and thus to predict the range of frequencies for which the SNR exceeds some particular value.

3. When using electromagnetic seismometers for recording low level seismic signals, it is essential that the coupling network to the operational amplifier–based preamplifier utilize as low values of resistance as possible (see Fig. 7). This can only be achieved by connecting the seismometer to the noninverting input or close coupling the seismometer directly to the inverting input. To minimize electronic noise, avoid connecting the seismometer to the inverting input of the operational amplifier through a large gain-setting input resistor. Also to be avoided is connecting the seismometer to the inverting input through the damping resistor, since this puts the coil and damping resistors in series rather than in parallel.

4. When using E-M seismometers with generator constants over several hundred V/m/sec, care must be taken to avoid increases in electronic noise due

to the back emf. This requires use of a FET-based operational amplifier unless the inverting configuration is used, which is usually not advantageous. Equation (B16) can be used to estimate how the back emf term $|Z_s|^2$ compares with R^2.

5. System noise tests of electromagnetic seismometer systems that clamp the seismometer mass or substitute a metal film resistor for the coil and damping resistor at the noninverting input of a preamplifier are likely to under estimate the system noise. The reason is that such tests eliminate the back emf term, which can be large for seismometers with large generator constants.

In addition there are a number of points which relate to the choice of parameters and type of components used in the design of seismometers.

6. In choosing an operational amplifier, compute the total input noise, equations (A12) and (A29), and select one that will minimize the noise for the source resistance being used. Include the back emf term where appropriate.

7. Unless the damping is uselessly low, electromagnetic seismometers to be used to record low-level seismic signals should have an inertial mass of at least 0.1 kg to avoid the degrading effect of suspension noise. Otherwise operation in a vacuum is necessary.

8. From equations (9) and (13), it is clear that the SNR for an electromagnetic seismometer is proportional to the square of the generator constant, G^2, over the entire frequency range, which is to be expected. For frequencies below the resonant frequency, f_0, the SNR is proportional to $1/f_0^4$. So, as is well known, it is desirable in choosing instrument parameters to maximize G and minimize f_0.

Acknowledgments

The author was motivated in this study by the extensive investigation of seismometer self-noise and frequency limits undertaken in connection with DOE's Deployable Seismic Verification System program. These measurements were carried out by the Sandia National Laboratories and USGS's Albuquerque Seismic Laboratory. Both laboratories generously supplied the results of their testing. The author is grateful to Jim O'Donnell of DOE and John Tsitouras of EGG for involving him in this program and for their encouragement and support of parts of this study.

Numerous individuals have contributed to the ideas developed here. The author is particularly indebted to H. B. (Jim) Durham, formerly of Sandia National Laboratories, for introducing him to the use of SNR in evaluating a seismometer and for discussions of the problems at the higher frequencies. Jon Peterson of USGS's Albuquerque Seismic Laboratory supplied his seismic LNM, which formed the basis for the paper. Bob Hutt of the same facility provided helpful data and information. The excellent paper by Riedesel *et al.* (1990) made the author aware of the subtle complexities of noise in operational amplifier circuits. Scott Swain of the Institute for Crustal Studies, University of California at Santa Barbara, provided useful information on the noise in operational amplifiers. Professor Tom McEvilly of the University of California at Berkeley provided continuous encouragement and moral support. The results of the Sandia National Laboratory noise tests on the GS-13 were supplied by Jim O'Donnell and Jim Durham.

Finally, the author would like to thank the Lawrence Livermore National Laboratory and his colleagues there, Keith Nakanishi and Phil Harben, both for support and for providing a SUN work station without which these computations could not have been made. And the author wishes to express appreciation also for the support of the computer personnel of the Treaty Verification Group, particularly Joe Tull for developing and providing the Seismic Analysis Code (SAC).

This work was partially supported by the Lawrence Livermore National Laboratory under DOE Contract W-7405-Eng-48.

References

Aki, K. and P. Richards (1980). *Quantitative Seismic Theory and Methods*, W. H. Freeman, San Francisco.

Aseltine, J. A. (1958). *Transform Method in Linear System Analysis*, McGraw-Hill, New York.

Berger, J., H. K. Eissler, F. L. Vernon, I. L. Neresov, M. B. Gokhberg, O. A. Stolyrov, and N. T. Tarasov (1988). Studies of high-frequency noise in eastern Kazakhstan, *Bull. Seism. Soc. Am.* **78**, 1744–1758.

Daniel, R. G. (1979). An intermediate-period field system using a short-period seismometer, *Bull. Seism. Soc. Am.* **69**, 1623–1626.

Gurrola, H., J. B. Minster, H. Given, F. Vernon, J. Berger, and R. Aster (1990). Analysis of high-frequency seismic noise in the Western United States and Eastern Kazakhstan, *Bull. Seism. Soc. Am.* **80**, 951-970.

Horowitz, P. and W. Hill. (1990). *The Art of Electronics*, Cambridge University Press, Cambridge.

Li, T. M. C., J. F. Ferguson, E. Herrin, and H. B. Durham (1984). High-frequency seismic noise at Lajitas, Texas, *Bull. Seism. Soc. Am.* **74**, 2015-2033.

Linear Technology Corporation (1990). *Linear Applications Handbook*, Design Note 15-1, Linear Technology Corporation, Milpitas, California.

Papoulis, A. (1965). *Probability, Random Variables, and Stochastic Processes*, McGraw-Hill, New York.

Peterson, J. (1982). GDSN Enhancement Studies Final Report, ARPA Order No. 4259, USGS Albuquerque Seismological Laboratory, Albuquerque, New Mexico, November.

Peterson, J. and C. Hutt (1982). *Test and calibration of the Digital World-Wide Standardized Seismograph U.S. Geol. Surv. Open-File Rep. 82-1087.*

Peterson, J. and C. Hutt (1989). *IRIS/USGS plans for upgrading the Global Seismographic Network, U.S. Geol. Surv. Open-File Rep. 89-471.*

Peterson, J. and E. T. Tilgner (1985). *Description and preliminary testing of the CDSN sensor systems, U.S. Geol. Surv. Open-File Rep. 85-288.*

Riedesel, M. A., R. A. Moore, and J. A. Orcutt (1990). Limits of sensitivity of inertial seismometers with velocity transducers and electronic amplifiers, *Bull. Seism. Soc. Am.* **80**, 1725–1752.

Roberts, P. M. (1989). A versatile equalization circuit for increasing seismometer velocity response below the natural resonant frequency, *Bull. Seism. Soc. Am.* **79**, 1607–1617.

Rodgers, P. W. (1975). A note on the nonlinear response of the pendulous accelerometer, *Bull. Seism. Soc. Am.* **65**, 523–530.

Rodgers, P. W. (1992). Frequency limits for seismometers as determined from signal-to-noise ratios. Part 2. The displacement feedback seismometer, *Bull. Seism. Soc. Am.* **82**, 1099–1123.

Rodgers, P. W., S. R. Taylor, and K. K. Nakanishi (1987). System and site noise in the Regional Seismic Test Network from 0.1 to 20 Hz, *Bull. Seism. Soc. Am.* **77**, 663–678.

Taylor, S. (1981). Properties of ambient seismic noise and summary of noise spectra in vicinity of RSTN sites, Lawrence Livermore National Laboratory, Livermore, California, UCID-18929.

Teledyne Geotech Corporation (1980). *Operation and Maintenance Manual, Preamplifier and Galvanometer Interface, Model 43310*, Teledyne Geotech Corporation, Garland, Texas.

Tobey, G. E., J. G. Graeme, and L. P. Huelsman (1971). *Operational Amplifiers: Design and Applications*, McGraw-Hill, New York.

Vergers, C. A. (1987). *Handbook of Electrical Noise and Technology*, Ed. 2, TAB Professional and Reference Books, TAB Books, Blue Ridge Summit, Pennsylvania.

Appendix A

This development of the expressions for noise in operational amplifiers was motivated by the treatment of the subject by Riedesel *et al.*, (1990). The material follows and expands on that treatment and results in different conclusions. This development refers all the noises back to the signal input terminals of the operational amplifier. The results significantly affect the way E-M seismometers should be connected to operational amplifier-based preamplifiers to maximize the SNR.

Noise in the Inverting Operational Amplifier

The standard inverting operational amplifier configuration is shown in Figure A1. All the variables are represented as power spectral densities (pds's). The noise current, I_{nn}, is shown as a Norton generator from the inverting input to ground, and the noise voltage as a Thevenin generator in series with the

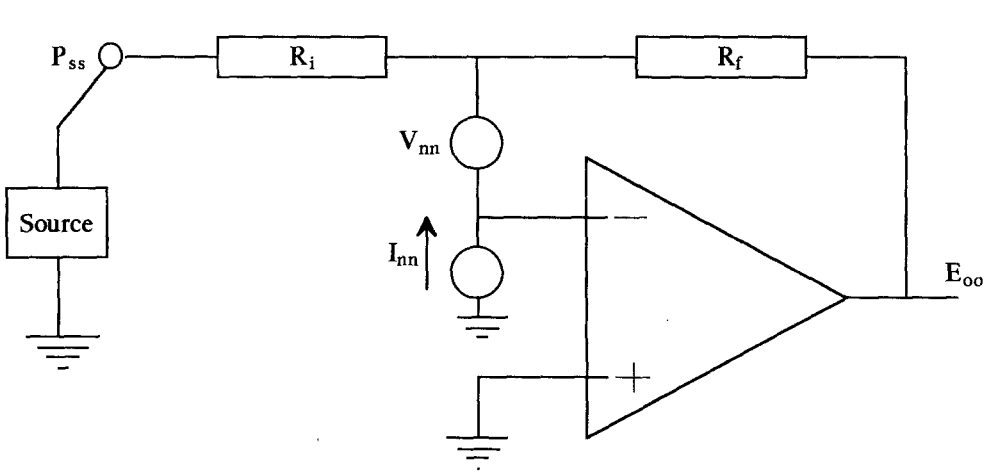

FIG. A1. The inverting amplifier configuration is shown. The gain setting resistors are R_i and R_f. All variables are pd's in V^2/Hz or A^2/Hz. V_{nn} and I_{nn} are the voltage noise and current noise pds's appearing at the terminals of the operational amplifier. P_{ss} is the input signal pds. E_{oo} is the output voltage noise pds due to all the noise sources. E_{nn} is the total electronic noise referred to the input, which is obtained by dividing E_{oo} by the square of the gain $(R_f/R_i)^2$. In order to obtain as low a noise as possible, there is no offset balancing resistor from the positive terminal to ground.

summing junction at the intersection of R_i and R_f. This is the model used by Tobey *et al.*, (1971) in their Appendix A. The total electronic noise referred to the input terminal is E_{nn}. The input signal pds is P_{ss} and the amplifier output is E_{oo}. Except when computing the SNR, P_{ss} will be zero. The procedure will be to compute E_{oo} for each noise source, and then refer it back to the input by dividing by the square of the gain for the inverting amplifier, $(R_f/R_i)^2$. Finally, all these noises referred to the input will be summed to obtain E_{nn}.

Voltage Noise

$E_{oo,v} = E_{oo}$ due to the voltage noise, V_{nn}. From the voltage divider relationship between V_{nn} and E_{oo}, $E_{oo,v}$ can be obtained as:

$$E_{oo,v} = \left[\frac{R_i + R_f}{R_i}\right]^2 V_{nn}. \tag{A1}$$

Dividing $E_{oo,v}$ by $(R_f/R_i)^2$ refers it to the input

$$E_{nn,v} = \frac{E_{oo,v}}{\left(\frac{R_f}{R_i}\right)^2}. \tag{A2}$$

Finally substituting equation (A1), $E_{nn,v}$ is obtained:

$$E_{nn,v} = \left[1 + \frac{R_i}{R_f}\right]^2 \cdot V_{nn}. \tag{A3}$$

Current Noise

$E_{oo,i} = E_{oo}$ due to noise current, I_{nn}. Because the left side of R_i is at ground through the source (which is turned off) and the right side is at vitual ground, there is no potential difference across R_i due to I_{nn}. Therefore, all of I_{nn} flows through R_f and none of it flows through R_i. Therefore,

$$E_{oo,i} = R_f^2 I_{nn}. \tag{A4}$$

Dividing by the gain squared to refer $E_{oo,i}$ to the input, there results

$$E_{nn,i} = \frac{R_f^2 I_{nn}}{\left(\frac{R_f}{R_i}\right)^2} = R_i^2 I_{nn}. \tag{A5}$$

What is surprising about equation (A5) is that, although I_{nn} does not flow through R_i, the gain action of the operational amplifier produces a term $R_i^2 I_{nn}$ in E_{nn}. To develop this further, it is useful to turn on the source and compute the SNR with I_{nn} as the only noise generator ($V_{nn} = 0$). The SNR at the input is then given by

$$\mathrm{SNR}_{\mathrm{input}} = \frac{P_{ss}}{E_{nn,i}} = \frac{P_{ss}}{R_i^2 I_{nn}}. \tag{A6}$$

The SNR at the output is obtained by multiplying P_{ss} by the gain squared and dividing by $R_f^2 I_{nn}$:

$$\mathrm{SNR}_{\mathrm{output}} = \frac{\left(\frac{R_f}{R_i}\right)^2 P_{ss}}{R_f^2 I_{nn}} = \frac{P_{ss}}{R_i^2 I_{nn}}. \tag{A7}$$

The SNR at the input and the output are seen to be equal, as they should be. The implication of equation (A6) and (A7) is that, when using an operational amplifier in the inverting configuration as a preamplifier for an E-M seismometer, it is important to keep R_i as low as possible to minimize noise and maximize the SNR. As this is difficult to do without loading the seismometer excessively, the noninverting configuration is to be preferred.

Johnson or Thermal Noise

$E_{oo,Ri} = E_{oo}$ due to Johnson noise generated by R_i. The Johnson noise generated by R_i is obviously in series with any source voltage, if one were present. Therefore,

$$E_{oo,Ri} = 4kTR_i\left(\frac{R_f}{R_i}\right)^2. \tag{A8}$$

Dividing by the gain squared refers $E_{oo,Ri}$ back to the input:

$$E_{nn,Ri} = 4kTR_i. \tag{A9}$$

$E_{oo,\,Rf} = E_{oo}$ due to Johnson noise generated by R_f. Since the left side of R_f is at vitual ground, it generates a component of E_{oo} directly:

$$E_{oo,\,Rf} = 4kTR_f. \tag{A10}$$

Dividing by the gain squared refers $E_{oo,\,Ri}$ back to the input:

$$E_{nn,\,Rf} = 4kT\frac{R_i^2}{R_f}. \tag{A11}$$

Finally summing up the four noise pd's at the input terminal,

$$E_{nn} = E_{nn,\,v} + E_{nn,\,i} + E_{nn,\,Ri} + E_{nn,\,Rf},$$

$$E_{nn} = \left[1 + \frac{R_i}{R_f}\right]^2 V_{nn} + R_i^2 I_{nn} + J_{nn1}, \tag{A12}$$

where

$$J_{nn1} = 4kTR_i\left(1 + \frac{R_i}{R_f}\right). \tag{A13}$$

Equations (A12) and (A13) are the complete equations for the total voltage referred to the input for the inverting operational amplifier.

To further simplify these expressions, for only moderately large gain R_i/R_f becomes negligible compared with one, and equations (A12) and (A13) simplify to

$$E_{nn} = V_{nn} + R_i^2 I_{nn} + J_{nn2}, \tag{A14}$$

where

$$J_{nn2} = 4kTR_i. \tag{A15}$$

Equation (A14) is equivalent to equation (6) in the body of the text where R plays the roll of R_i. This also corrects Linear Technology Corporation (1990), in which I_{nn} is shown flowing through the parallel combination of R_i and R_f.

Noise in the Noninverting Operational Amplifier

The standard noninverting operational amplifier configuration is shown in Figure A2. All the variables are represented as pds's. The noise currents, I_{nn-} and I_{nn+}, are shown as Norton generators from the inverting and noninverting inputs to ground. The noise voltage is shown as a Thevenin generator in series with the summing junction at the intersection of R_i and R_f. This is the model used by Tobey *et al.*, (1971). The total electronic noise referred to the input terminal is E_{nn}. The input signal pds is P_{ss} and the amplifier output is E_{oo}. The analysis procedure will be the same as that used for the inverting operational amplifier. The square of the standard gain for the noninverting amplifier is $(1 + R_f/R_i)^2$.

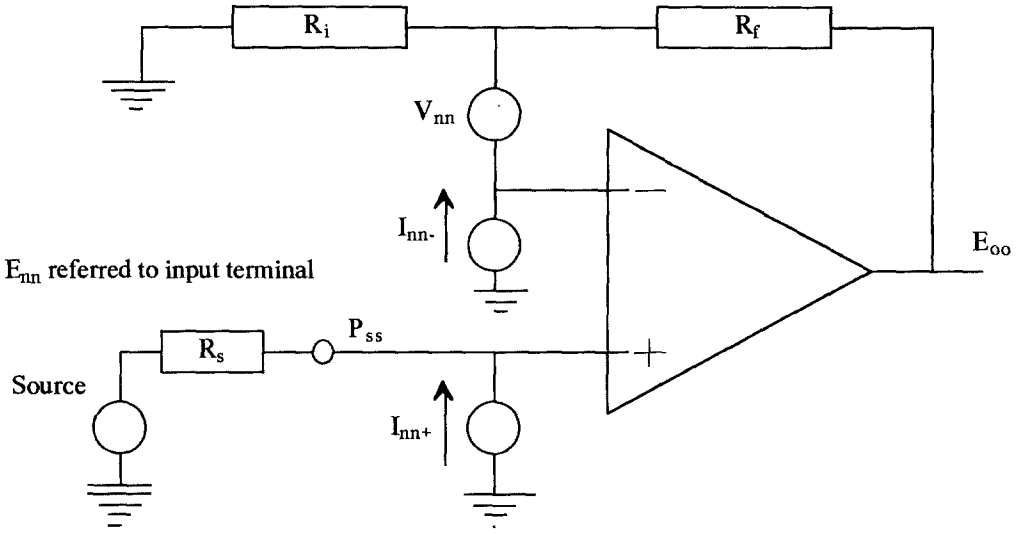

FIG. A2. The noninverting amplifier configuration is shown. The gain setting resistors are R_i and R_f. R_s is the source resistance. All variables are pds's in V^2/Hz or A^2/Hz. V_{nn}, I_{nn-}, and I_{nn+} are the voltage noise and current noise pds's appearing at the terminals of the operational amplifier. P_{ss} is the input signal pds. E_{oo} is the output voltage noise pds due to all the noise sources. E_{nn} is the total electronic noise referred to the input, which is obtained by dividing E_{oo} by the square of the gain, $(1 + R_f/R_i)^2$.

Voltage Noise

$E_{oo,v} = E_{oo}$ due to the voltage noise, V_{nn}. From the voltage divider relationship between V_{nn} and E_{oo}, $E_{oo,v}$ can be obtained as

$$E_{oo,v} = \left[\frac{R_i + R_f}{R_i}\right]^2 V_{nn}. \tag{A16}$$

Dividing by the gain squared results in

$$E_{nn,v} = V_{nn}. \tag{A17}$$

Current Noise

$E_{oo,i} = E_{oo}$ due to noise current, I_{nn-}. Because the left side of R_i is at ground and the right side is at virtual ground, there is no potential difference across R_i due to I_{nn-}. Therefore, all of I_{nn-} flows through R_f, and none of it flows through R_i. Therefore,

$$E_{oo,i-} = R_f^2 I_{nn}. \tag{A18}$$

Dividing by the gain squared results in

$$E_{nn,i-} = \left[\frac{R_f R_i}{R_f + R_i}\right]^2 I_{nn-}. \tag{A19}$$

$E_{oo,i+} = E_{oo}$ due to noise current, I_{nn+}. I_{nn+} flows directly through the source resistance, R_s. Therefore, $E_{nn,i+}$ is given directly by

$$E_{nn,i+} = R_s^2 I_{nn+}. \tag{A20}$$

Johnson or Thermal Noise

$E_{oo,\,Ri} = E_{oo}$ due to Johnson noise generated by R_i. The Johnson noise generated by R_i is obviously in series with any source voltage, if one were connected to the left side of R_i. Therefore, following the method used for the inverting amplifier, $E_{oo,\,Ri}$ is found to be given by

$$E_{oo,\,Ri} = 4kTR_i\left(\frac{R_f}{R_i}\right)^2. \tag{A21}$$

To refer to the input divide by the squared gain to obtain

$$E_{nn,\,Ri} = 4kTR_i \cdot \left[\frac{1}{1 + \dfrac{R_i}{R_f}}\right]^2. \tag{A22}$$

$E_{oo,\,Rf} = E_{oo}$ due to Johnson noise generated by R_f. Since the left side of R_f is at virtual ground, it generates a component of E_{oo} directly:

$$E_{oo,\,R_f} = 4kTR_f. \tag{A23}$$

Dividing by the gain squared refers $E_{oo,\,Ri}$ back to the input:

$$E_{nn,\,Rf} = 4kTR_f \cdot \left[\frac{1}{1 + \dfrac{R_f}{R_i}}\right]^2. \tag{A24}$$

$E_{nn,\,Rs} = E_{nn}$ due to Johnson noise generated by R_s. The Johnson noise generated by R_s is obviously in series with the Thevenin source voltage. Therefore,

$$E_{nn,\,Rs} = 4kTR_s. \tag{A25}$$

Finally, summing up the six noise pds's at the input terminal:

$$E_{nn} = E_{nn,\,v} + E_{nn,\,i-} + E_{nn,\,i+} + J_{nn3}, \tag{A26}$$

where

$$J_{nn3} = 4kTR_i \cdot \left[\frac{1}{1 + \dfrac{R_i}{R_f}}\right]^2 + 4kTR_f \cdot \left[\frac{1}{1 + \dfrac{R_f}{R_i}}\right]^2 + 4kTR_s. \tag{A27}$$

Equations (26A) and (27A) are the complete equations for the total voltage noise referred to the input for the noninverting operational amplifier.

To further simplify these expressions, for only moderately large gain R_i/R_f becomes negligible compared with one, so $1 + R_f/R_i = R_f/R_i$. It is also

reasonable to assume that the current noises at the inverting and noninverting inputs have the same pds's. Therefore;

$$I_{nn-} = I_{nn+} = I_{nn}. \tag{A28}$$

With these assumptions, equations (A26) and (A27) simplify to

$$E_{nn} = V_{nn} + \left[R_s^2 + \left(\frac{R_f R_i}{R_f + R_i} \right)^2 \right] I_{nn} + J_{nn4}, \tag{A29}$$

where

$$J_{nn4} = 4kT \left(\frac{R_f^2}{R_i} + \frac{R_i^2}{R_f} + R_s \right). \tag{A30}$$

In the body of the paper, it is assumed that, when using the noninverting operational amplifier, the gain setting resistors are kept to such a low value that they are negligible compared to the source resistance, R_s. As discussed, this may be difficult to achieve in practice, but it serves as a useful limiting case in this noise study. Based on this, replace R_s with the equivalent source resistance, R, used in the body of the paper ($R_s = R$). So the final expression for E_{nn} becomes

$$E_{nn} = V_{nn} + R^2 I_{nn} + J_{nn}, \tag{A31}$$

where J_{nn} is given by equation (A30).

Appendix B

Noise Voltage due to Noise Current including the Seismometer Motion: A Derivation of the Expression for $|Z_s|^2$ in Equation (6)

As explained in the section on electronic noise models, a noninverting operational amplifier has several noise sources, one of which is a noise current which flows from the positive terminal of the operational amplifier into the seismometer. The result is that the total voltage noise pds is given by equation (6), which is repeated here with $|Z_s|^2$ substituted for R^2:

$$E_{nn} = V_{nn} + J_{nn} + I_{nn} |Z_s|^2. \tag{6}$$

The reason for substituting $|Z_s|^2$ for R^2 will now be developed. In this study, the idealized noise situation is assumed in which the input resistances associated with the operation amplifier(s) are all small compared to the seismometer resistances. Therefore, the noise voltage, v_i, due to the noise current, i_n, is produced by i_n flowing through the seismometer. This only happens when the operational amplifier is in the noninverting configuration.

The circuit is shown in Figure B1. In the left-hand figure, the noise current, i_n, flows into the seismometer coil and damping resistances, r_c and r_d, respectively. The part of i_n that flows through r_c produces a force on the seismometer mass causing the mass to move and generate a back emf eg. G is the open circuit generator constant defined for equation (9) earlier, and z is the relative motion of the mass with respect to the frame of the seismometer. All the

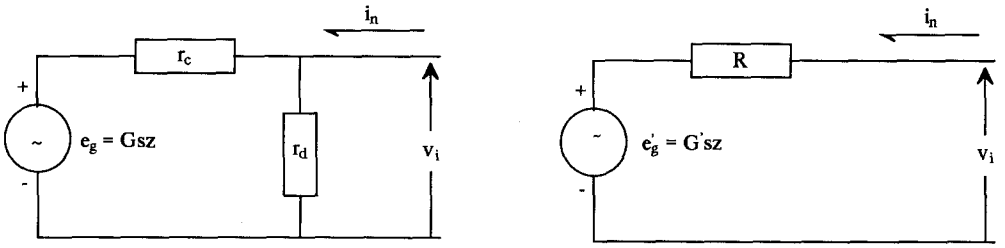

FIG. B1. On the *left* is the seismometer output circuit showing noise current input, i_n, the coil and damping resistances, r_c and r_d, respectively, and the back emf, e_g, generated by the motion of the seismometer mass. The resulting noise voltage due to i_n is v_i. G is the unloaded generator constant. The right hand circuit is the Thevenin equivalent of the left-hand circuit.

variables are Laplace transformed, so sz is the transform of the relative mass velocity. To simplify the analysis, the left-hand circuit is replaced by its Thevenin equivalent shown on the right. R is the parallel resistance of r_c and r_d, and G' is the effective or loaded constant. R and G' ar given by equations (B1) and (B2):

$$R = \frac{r_c r_d}{r_c + R_d} \qquad \text{(ohms)}, \tag{B1}$$

$$G' = \frac{r_d}{r_c + r_d} \cdot G \qquad \text{(V/m/sec)}. \tag{B2}$$

The noise voltage resulting from i_n flowing through the equivalent seismometer is

$$v_i = i_n R + e'_g \qquad \text{(volts)}, \tag{B3}$$

where

$$e'_g = G' sz \qquad \text{(volts)}. \tag{B4}$$

The motion of the seismometer mass due to the force produced by i_n is given by

$$(Ms^2 + Bs + K)z = f_i, \tag{B5}$$

where M, B, and K are the seismometer mass, damping, and spring constant, respectively, and the force, f_i, is given by

$$f_i = G' i_n \qquad \text{(Newtons)}. \tag{B6}$$

Dividing equation (B5) through by M allows it to be put in the standard form:

$$(s^2 + 2\zeta\Omega s + \Omega^2)z = \frac{f_i}{M}, \tag{B7}$$

where ζ and Ω in equation (B7) were defined in the body of the paper.

The complex impedance for the seismometer, including the back emf due to mass motion, is found from equation (B8):

$$Z_s = \frac{v_i}{i_n} \qquad \text{(ohms)}. \tag{B8}$$

With some manipulation, Z_s is found using equations (B1) through (B7):

$$Z_s = \left(R + \frac{1}{M}\left[\frac{r_d}{r_c + r_d} G\right]^2 \cdot \frac{s}{s^2 + 2\zeta\Omega s + \Omega^2} \right) \quad \text{(ohms)}. \tag{B9}$$

motional impedance, Z_m

The second term in the parenthesis is due to the motion of the mass and is termed the motional impedance, Z_m. If the seismometer mass is held motionless, or clamped, $G = 0$ and Z_s degenerates to

$$Z_s = R. \tag{B10}$$

The term being soughts is $|Z_s|^2$, which is found by setting $s = i\omega$ in equation (B9) and using

$$|Z_s|^2 = Z_s Z_s^* \qquad (\text{ohms}^2). \tag{B11}$$

After considerable manipulation, this results in the desired expression:

$$|Z_s|^2 = \left\{ \left[R + \frac{2\zeta\Omega}{M} |H(\omega)|^2 \right]^2 + \left[\frac{1}{M\omega} (\Omega^2 - \omega^2) |H(\omega)|^2 \right]^2 \right\}, \tag{B12}$$

where $|H(\omega)|^2$ was defined by equation (9) in the body of the paper and is repeated here:

$$|H(\omega)|^2 = \left[\frac{r_d}{r_c + r_d} G \right]^2 \cdot \frac{\omega^2}{(\Omega^2 - \omega^2)^2 + 4\zeta^2\Omega^2\omega^2}. \tag{B13}$$

Two limiting cases for $|Z_s|^2$ are of interest. The first is when the mass is clamped, which was treated earlier for Z_s. For a clamped mass, $G = 0$, and equation (B12) degenerates to

$$|Z_s|^2 = R^2, \tag{B14}$$

and equation (6) becomes the conventional expression for total electronic noise in the noninverting case:

$$E_{nn} = V_{nn} + J_{nn} + I_{nn} R^2. \tag{B15}$$

The other limiting case of interest is the expression for $|Z_s|^2$ at resonance. Setting $\omega = \Omega$, equation (B12) simplifies to

$$|Z_s|^2_{\max} = |Z_s|^2_{\omega=\Omega} = \left[R + \frac{1}{2\zeta\Omega M} \cdot \frac{r_d}{r_c + r_d} G \right]^2. \tag{B16}$$

As indicated, this is also the maximum value for $|Z_s|^2$. This expression is useful in estimating if there is going to be a problem in ignoring the motional resistance in a particular seismometer-operational amplifier-resistor configuration.

In Figure B2, the size of $|Z_s|^2$ is compared to R^2 for the GS-13 and L-4C electromagnetic seismometers. The upper curve and line are for the GS-13 and

the lower pair for the L-4C. The horizontal lines are the values for $|Z_s|^2$ for each instrument with their masses clamped. The increase in $|Z_s|^2$ over the clamped mass value, R^2, is much greater for the GS-13 than for the L-4C because of its greater generator constant. This results in a larger motional impedance, Z_m, for the GS-13. For both instruments, the $|Z_s|^2$ curves peak at their 1-Hz resonances, as indicated by equation (B16).

Figure B3 shows the total electronic noise, E_{nn}, for each seismometer with its mass clamped and unclamped. The data were computed using equations (6) and (B12). The current and voltage noise models used are those for the OP-27 operational amplifier. As before, the upper two curves are for the GS-13 and the lower two for the L-4C. The two unpeaked curves are the total electronic noises with the masses clamped. Notice that for the GS-13, the actual unclamped electronic noise, E_{nn}, exceeds the clamped by two orders of magnitude at 1 Hz. These data confirm that clamped mass tests run on systems having seismometers with large generator constants, such as the GS-13, S-13, and L-4C, will tend to underestimate the system noise when a noninverting configuration is used. This is particularly true when bipolar operational amplifiers such as the OP-27 are used.

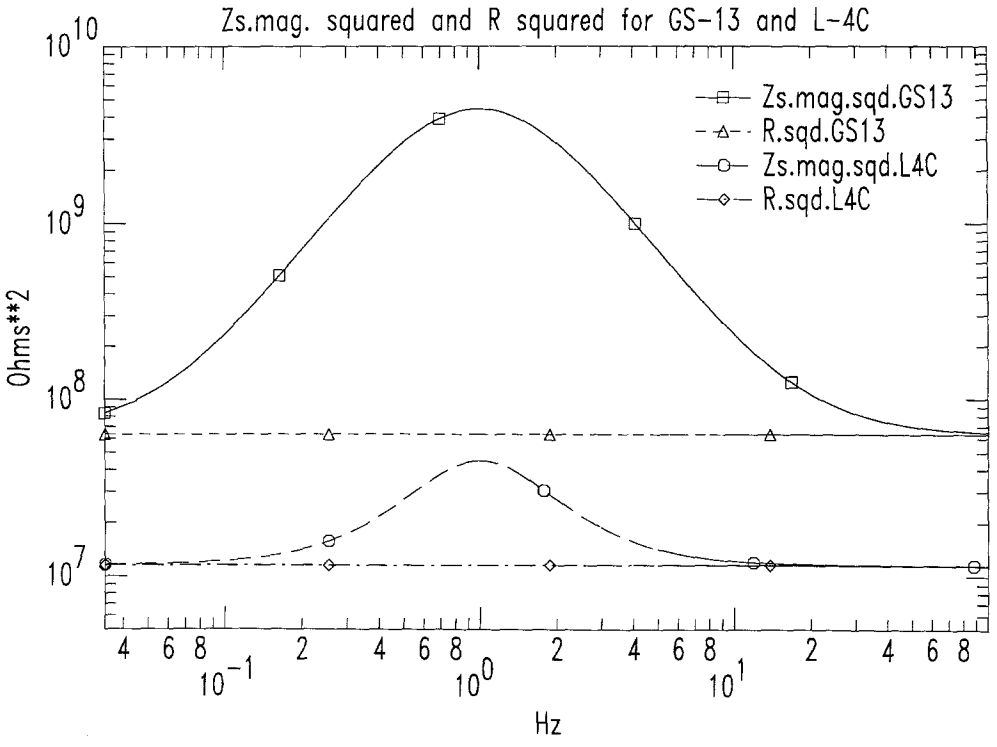

FIG. B2. This figure compares seismometer motional and resistive impedances squared for the GS-13 and L-4C with clamped and unclamped masses. The noninverting configuration was used. The upper curve and the line are for the GS-13, and the lower pair is for the L-4C. The two peaked curves are the square of the magnitude of the motional impedances, $|Z_s|^2$, for each seismometer with the masses unclamped. They are larger than the resistances squared alone, the two horizontal lines, because of the apparent motional impedance produced by the back electro-motive-force generated by the motion of the mass of each seismometer. The mass motion is induced by the noise current, i_n, from the operational amplifier.

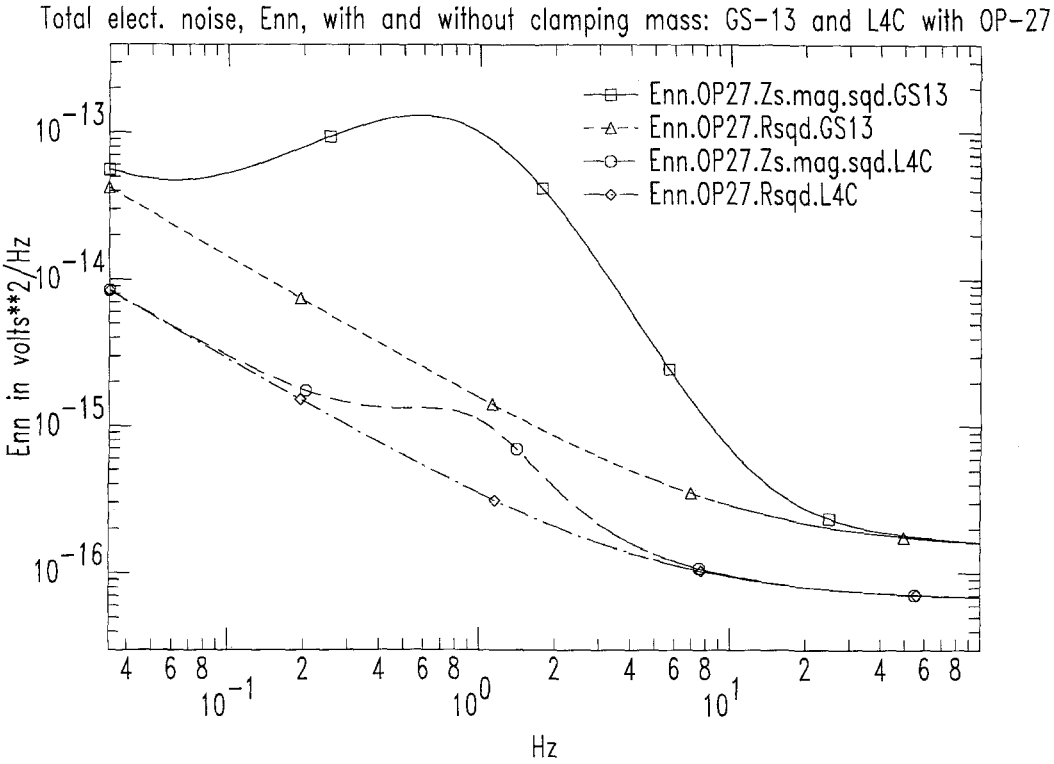

FIG. B3. The total electronic noise, E_{nn}, for the GS-13 and L-4C seismometers with the OP-27 operational amplifier is shown. The noninverting configuration was used. The upper pair of curves is for the GS-13, and the lower pair for the L-4C. The two peaked curves give E_{nn} for unclamped masses, and the lower unpeaked curves for clamped masses. These data show the possibility of under estimating system noise in clamped mass tests of systems using seismometers with large generator constants and bipolar operational amplifiers.

INSTITUTE FOR CRUSTAL STUDIES
UNIVERSITY OF CALIFORNIA
SANTA BARBARA, CALIFORNIA 93106-1100

LAWRENCE LIVERMORE NATIONAL LABORATORY
L-205
P.O. BOX 808
LIVERMORE, CALIFORNIA 94550

Manuscript received 26 July 1991